

Sub-shot noise sensitivity via deformed four-headed kitten states

Naeem Akhtar,¹ Xiaosen Yang,^{1,*} Jia-Xin Peng,^{2,†} Inaam Ul Haq,³ Yuee Xie,¹ and Yuanping Chen^{1,‡}

¹*Department of Physics, Jiangsu University, Zhenjiang, 212013, China*

²*School of Physics and Technology, Nantong University, Nantong, 226019, China*

³*Department of Physics, COMSATS University Islamabad, Islamabad Campus, 45550, Pakistan*

(Dated: December 3, 2024)

We explore nonclassical effects in the phase space of a four-headed kitten state (a superposition of two Schrödinger kitten states) induced by photon addition and subtraction operations applied in different sequences. We investigate two scenarios: in the first, photon addition is applied to the state, followed by photon subtraction, while in the second, the order of operations is reversed. We demonstrate that applying multiphoton operations to the state results in notable nearly isotropic sub-Planck structures, with the characteristics of these structures being influenced by the photon addition and subtraction. We observe that adding photons increases the average photon number, while photon subtraction reduces it in the first case but has no effect in the second. Increasing the number of added photons compresses the sub-Planck structures in both cases. Photon subtraction, however, has the opposite effect on the sub-Planck structures in the first case and no effect in the second, although it may improve their isotropy at optimal settings. The presence of the sub-Planck structures in our states leads to improved sensitivity to displacements, exceeding the standard quantum limit, as verified across all the depicted scenarios.

I. INTRODUCTION

Coherent states were first introduced by Schrödinger in 1926 [1, 2], and the concept was further developed in quantum optics by Glauber in 1963 [3]. Quantum superposition phenomena have been intensively investigated within the framework of the harmonic oscillator, leading to the creation of intriguing nonclassical states [4, 5]. The nonclassical nature of quantum states is revealed through nonclassical phase-space features, often visualized using the Wigner function [6, 7]. Nonclassical states are considered valuable resources for continuous variable quantum information processing, particularly for sensing and metrology applications [8–12]. A critical factor in determining the utility of a quantum state for such applications is the degree to which it becomes distinguishable from the initial state after a small displacement, which is influenced by the smallest phase-space feature of a quantum state and measures sensitivity to displacement (perturbation) [13–15]. Developing quantum states with finer phase-space features is essential for enhancing their capacity to measure smaller scale displacements, and quantum states with finer phase-space features are highly valuable for advancing quantum measurement techniques and improving the performance of quantum technologies [16].

The phase-space volume occupied by a coherent state adheres to the Planck scale \hbar [17], while also preserving its sensitivity to displacements at this standard limit [18, 19]. It has been shown that specific chaotic quantum systems [13, 20] are able to produce phase-space features with volumes far below this standard norm. A

macroscopic cat state [21, 22], which is the superposition of two distinct coherent states, is a prominent example of nonclassical states and has shown more finer phase-space features and greater sensitivity compared to a coherent state [23]. The notion of coherent-state superpositions has been evolved to a generalized form of macroscopic cat states [11, 13, 24, 25]. Compass states [13, 23, 25–38] (a superposition of four coherent states) have been shown to exhibit improved phase-space characteristics compared to their precursors, namely coherent states and cat states. In particular, it has been found that these states hold sub-Planck scale features (dimension below than the Planck scale) and hold sensitivity to displacements greater than the standard quantum limit, which make them a potential candidate for quantum metrology applications [39]. Both theoretical [40–44] and experimental [45–48] approaches have been employed to generate catlike states.

Multiphoton operations applied to a quantum state provide innovative techniques for controlling fundamental nonclassical characteristics [49–60]. For example, it has been shown that photon subtraction (or addition) from ordinary squeezed-vacuum states may develop quantum states similar to those of cat states [50, 52, 53, 58]. In this work, we consider a four-headed kitten state, which is the superposition of two kitten states deficient in nonclassical phase-space attributes. Photon addition and subtraction operations are applied on this state in different orders to build new quantum states, which exhibit intriguing phase-space characteristics similar to a compass state [13]. In our first case, we apply photon addition followed by photon subtraction to the state, while in the second case, the order of operations is reversed, with photon subtraction applied first and then photon addition.

Our investigation utilizes phase-space formalism [7], incorporating Wigner function analysis and photon num-

* yangxs@ujs.edu.cn

† 18217696127@163.com

‡ chenyp@ujs.edu.cn

ber distributions. We compare the states to explore the effects of multiphoton operations and the optimal selection of parameters, followed by an analysis of their sensitivity to displacements. The analysis concludes with a thorough discussion of the physical significance and implications of each scenario. Specifically, we show that multiphoton operations applied on the four-headed kitten state lead to quantum states with refined phase-space characteristics, and interestingly, our proposed cases also hold sub-Planck phase-space features whose occurrence is now affiliated with the number of added and subtracted photons. Furthermore, we show that our proposed instances hold sensitivity to phase-space displacements greater than the standard quantum limit, making them a promising choice for quantum sensing applications. Our observations indicate that as the number of added photons increases, finer sub-Planck structures develop in our cases. Conversely, photon subtraction in the first scenario causes the sub-Planck structures to expand. In the second scenario (subtraction followed by addition), photon subtraction becomes ineffective, but in this case, an improvement in the isotropy (directional invariance in phase space) of the sub-Planck structures is observed for certain photon subtraction choices. These findings align with the behavior observed in the sensitivity of our quantum states.

Our paper is structured as follows: §II reviews the basics of sub-Planck structures and their impact on sensitivity to displacement, illustrated with the Zurek compass state. §III discusses deformed coherent states and our proposed quantum states, offering a detailed analysis to identify the corresponding phase-space characteristics. §IV presents phase-space sensitivity contained by our proposed quantum states. §V provides a compact summary of our findings, and §VI provides the main conclusions of our results.

II. CONCEPTS AND PERSPECTIVES

The quantum uncertainty principle for position and momentum, expressed through the commutation relation $[\hat{x}, \hat{p}] := i\hbar$ with \hat{x} and \hat{p} being the position and momentum operators, respectively, imposes constraints on the dimension of a phase-space structure. Specifically, it dictates that the product of the uncertainties in position (Δx) and momentum (Δp) satisfies $\Delta x \Delta p \geq \hbar/2$ [18, 19]. This implies that the dimension of a phase-space feature is constrained by this standard limit; if a phase-space feature has dimensions below this threshold, it is considered unphysical. This general assumption is challenged by Zurek [13], who demonstrates that the sub-Planck structures in the compass state significantly influence the phase-space properties of the states. These spotty features have been found crucial in enhancing sensitivity to displacements, and this improvement in sensitivity is directly dedicated to the sub-Planck scale structures in the state. In this section, we primarily focus on review-

ing the key concept of sub-Planck structures and their critical role in enhancing sensitivity to displacements.

A. Phase space and sensitivity

A Schrödinger coherent state can be expressed as a displaced vacuum state $|\alpha\rangle := \hat{D}(\alpha)|0\rangle$ with $\hat{D}(\alpha) := \exp(\alpha\hat{a}^\dagger - \alpha^*\hat{a})$ the displacement operator [61], where $\alpha \in \mathbb{C}$, and \hat{a} (\hat{a}^\dagger) are annihilation (creation) operators. Coherent states are the most classical pure states of light [17], but their superposition may exhibit nonclassical aspects due to quantum interference [62]. The Wigner function denoted by $W_{\hat{\rho}}(\boldsymbol{\beta})$ with $\boldsymbol{\beta} := (x, p)^\top$ constitutes phase space of a quantum state $\hat{\rho}$ [7], where x and p are the position and momentum pairs, respectively.

The Wigner function is one of the primary tools for analyzing the nonclassical characteristics of a quantum state [7]. Mathematically, the Wigner function can also be expressed as [63]

$$W_{\hat{\rho}}(\boldsymbol{\beta}) := \frac{e^{2|\boldsymbol{\beta}|^2}}{\pi^2} \int d^2\gamma \langle -\gamma | \hat{\rho} | \gamma \rangle e^{-2(\boldsymbol{\beta}^* \boldsymbol{\gamma} - \boldsymbol{\beta} \boldsymbol{\gamma}^*)}. \quad (1)$$

Note that dimensionless versions of the position and momentum operators are employed throughout this work.

The Schrödinger cat state is the superposition of two distinguishable coherent states, and one of the simplest examples of such states is the even cat state [64], which is denoted as

$$|\psi\rangle := \frac{1}{(2 + 2e^{-2|\alpha|^2})^{1/2}} [|\alpha\rangle + |-\alpha\rangle]. \quad (2)$$

A cat state is visible when the parameter α is high enough to maintain the orthogonality criterion $\langle \alpha | -\alpha \rangle \approx 0$. If the constituent coherent states in this superposition are not distinguishable, the resulting states is known as Schrödinger-kitten states [52].

We now discuss the concept of sensitivity to phase-space displacement. For a pure quantum state $|\psi\rangle$, this sensitivity can be mathematically determined by evaluating the overlap function between a quantum state and its slightly displaced version. This involves calculating how much one state resembles another when displaced in phase space, which provides insight into how precisely the quantum state can detect or respond to changes in its phase-space configuration. Mathematically, this sensitivity can be determined by using [14]

$$S_{|\psi\rangle}(\delta) := \int \frac{d^2\beta}{\pi} W_{|\psi\rangle}(\beta) W_{|\psi'\rangle}(\beta) = |\langle \psi | \psi' \rangle|^2 \quad (3)$$

with $|\psi'\rangle := \hat{D}(\delta)|\psi\rangle$. If $S_{|\psi\rangle}(\delta) = 0$, then a state and its displaced counterpart are orthogonal for the displacement δ . The overlap $S_{|\psi\rangle}(\delta)$ with $\delta := (\delta x, \delta p)^\top$, where δx and δp are values of the displacements applied along x and p directions in the phase space, respectively. The

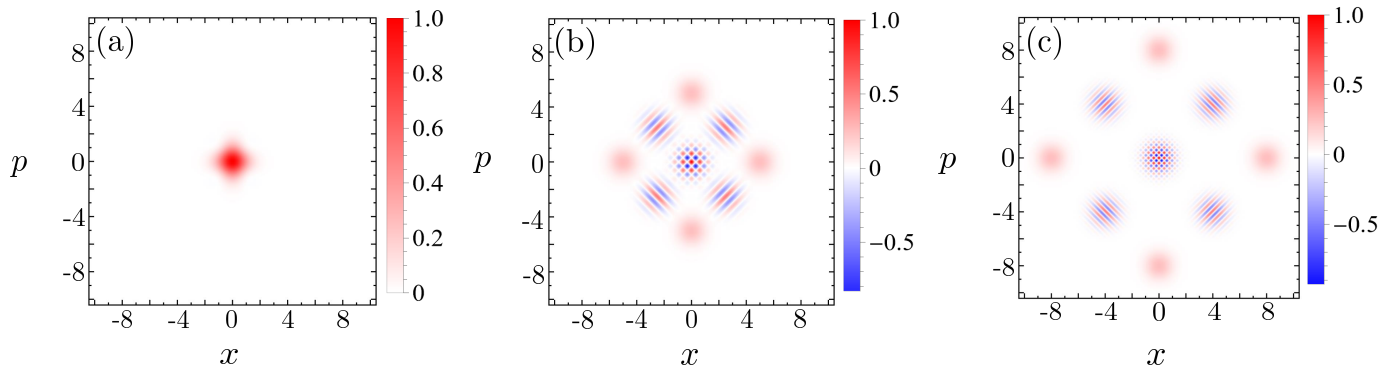


FIG. 1. The Wigner function of the compass state. (a) $c_0 = 1$, (b) $c_0 = 5$, and (c) $c_0 = 8$.

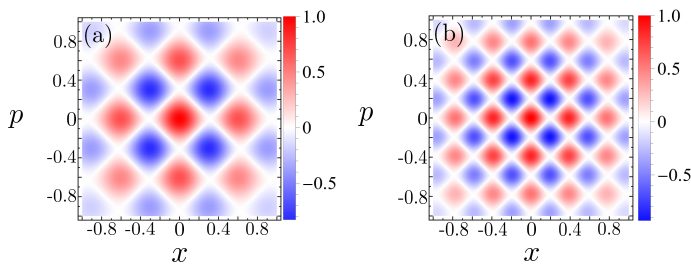


FIG. 2. Central interference of the compass state. (a) $c_0 = 5$ and (b) $c_0 = 8$.

infinitesimal perturbation δ , which makes the perturbed state quasi-orthogonal with the initial, provides information on the sensitivity to displacements. Smaller values of δ indicate greater sensitivity to displacements. This concept can be understood by considering a scenario where a signal intended for detection is linearly coupled to a harmonic oscillator. The oscillator measures a displacement that is proportional to the strength of the signal. In this context, the sensitivity of the oscillator to these displacements directly impacts its capacity to resolve the signal. Thus, quantum states with higher sensitivity are capable of detecting weaker signals with greater precision [26].

The Wigner function of a macroscopic cat state typically manifests as two distinct Gaussian peaks in phase space with an oscillatory interference pattern, where each peak corresponds to a coherent state; this quantum state is simply called a macroscopic cat state [65, 66]. In contrast, for a compass state, the Wigner function now holds four Gaussian peaks, a catlike interference pattern, and central sub-Planck structures [13], may also be classified as a four-component cat state [66, 67], aligning with the concept of multichotomous cat states [24]. Cat states, such as the one presented in Eq. (2), do not exhibit sub-Planck features as their interference phase-space features are not limited in all directions of phase space [23].

B. Sub-Planckian sensitivity

The Wigner function of a coherent state is denoted as

$$W_{|\alpha\rangle}(\beta) := e^{-2(\alpha-\beta)(\alpha^*-\beta^*)}, \quad (4)$$

which exhibits Gaussian form; hence, coherent states are types of Gaussian and nonclassical quantum states [17]. Moreover, the phase-space structure of a coherent state follows the minimal limit set by the uncertainty principle, often referred to as the Planck action in phase space. This implies that phase-space size of a coherent sets the minimal norm, and the sub-Planck structure is below this limit and can be limited as much as desired by varying the controlling parameter, whereas all of these characteristics are missing in the coherent [23].

The sensitivity of a coherent state to displacements in phase space is described by the function $S_{|\alpha\rangle}(\delta) := e^{-|\delta|^2}$. This overlap tends to zero for the displacement $|\delta| > 1$, implying that the sensitivity of a coherent state falls at the standard limits. The phase-space structure of a coherent state and its sensitivity adhere precisely to the standard quantum mechanical limits. This means that the coherent state achieves the theoretical minimum uncertainty allowed by the Heisenberg uncertainty principle, reflecting the optimal balance between precision in position and momentum measurements. Consequently, in our analysis, we evaluate each example by comparing it against these established norms. This involves assessing how each example measures up to the theoretical benchmarks and standard limits, allowing us to understand their relative performance and behavior in relation to these reference points.

We now include the example of the Zurek compass state [13], which is recognized as a superposition of coherent states given by $\alpha_1 = c_0/\sqrt{2}$, $\alpha_2 = -c_0/\sqrt{2}$, $\alpha_3 = ic_0/\sqrt{2}$, and $\alpha_4 = -ic_0/\sqrt{2}$, with $c_0 \in \mathbb{R}^+$. This superposition can also be interpreted as the superposition of two cat states, or equivalently as the superposition of four coherent states and is denoted as

$$|\diamond\rangle := N_{\diamond}^{-1/2} \sum_{i=1}^4 |\alpha_i\rangle, \quad (5)$$

where

$$N_{\diamond} = \sum_{i,j=1}^4 G_{\alpha_i, \alpha_j} e^{\alpha_i^* \alpha_j} \quad (6)$$

with

$$G_{k,l} := \exp \left[-\frac{1}{2} \{ |k|^2 + |l|^2 \} \right] \quad (7)$$

represents the normalization coefficient.

The Wigner function of the compass state $|\diamond\rangle$ is obtained as

$$W_{|\diamond\rangle}(\beta) = \frac{1}{N_{\diamond}} \sum_{i,j=1}^4 W_{|\alpha_i\rangle\langle\alpha_j|}(\beta) \quad (8)$$

with

$$W_{|\alpha_i\rangle\langle\alpha_j|}(\beta) := G_{\alpha_i, \alpha_j} \exp \left[-\alpha_i \alpha_j^* - 2(|\beta|^2 - \alpha_j^* \beta - \alpha_i \beta^*) \right]. \quad (9)$$

We present $W_{|\diamond\rangle}(\beta)$ in Fig. 1 for a few c_0 values. As depicted in Fig. 1(a), for $c_0 = 1$, the four coherent states in the compass state cannot be distinguished individually; hence, the corresponding Wigner distribution shows a central positive peak. This scenario represents the four-component kitten state, or alternatively may also be referred to as a four-headed kitten state [66]. However, for $c_0 = 5$, these four coherent states are now well separated and appear as four Gaussian lobes in the phase space, and the interference pattern is now pronounced in the phase space, as shown in Fig. 1(b). Figure 1(c) shows that increasing the macroscopic parameter to $c_0 = 8$ causes coherent states to be pushed further away from the phase-space origin, resulting in enhanced negative regions in the intensity plot. Figure 2 illustrates the central interference pattern of each case presented in Fig. 1, where the phase-space features are arranged in a tiled format. Each tile in this pattern has an extension considerably smaller than that of a coherent state, indicating that these structures are at the sub-Planck scale. Furthermore, as c_0 increases, the size of the sub-Planck features decreases.

The enhancement in sensitivity for a cat state is limited to a particular direction in the phase space. Consequently, compass states are deemed more advantageous than cat states as they may offer greater sensitivity [23]. The overlap between the compass state $|\diamond\rangle$ and its displaced version $\hat{D}(\delta)|\diamond\rangle$ reflects the sensitivity to displacement in phase space,

$$S_{\diamond}(\delta) = \left| \sum_{i,j=1}^4 O_{|\alpha_i\rangle\langle\alpha_j|}(\delta) \right|^2, \quad (10)$$

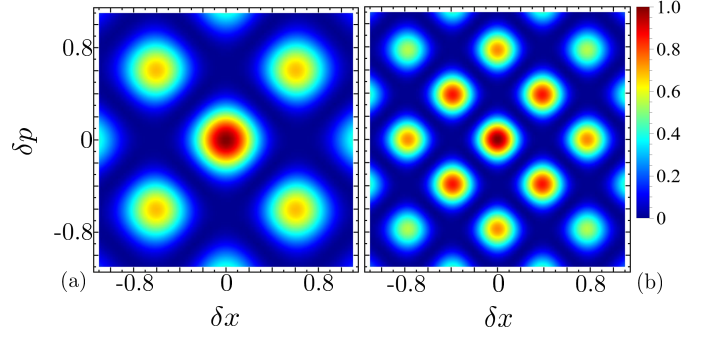


FIG. 3. The overlap between the compass state and its displaced versions, represented by $S_{\diamond}(\delta)$, quantifies the corresponding sensitivities over given parameters chosen with (a) $c_0 = 5$ and (b) $c_0 = 8$. The intensity plots are normalized to unity for each case.

where

$$O_{|\alpha_i\rangle\langle\alpha_j|}(\delta) := G_{\alpha_i, \alpha_j} \exp \left[\alpha_i^* \alpha_j + \alpha_i^* \delta - \alpha_j \delta^* - \frac{|\delta|^2}{2} \right]. \quad (11)$$

Note that we skip normalization for the sensitivity cases as their intensity visualizations are already normalized to unity. Figures 3(a) and (b) show that the overlap function $S_{\diamond}(\delta)$ is zero for $|\delta| < 1$, with $c_0 = 5$ and $c_0 = 8$ in the respective cases involving the sub-Planck structures. This means that the sensitivity to displacement for this compass state is enhanced as compared to a coherent state. Furthermore, compared to the coherent state, the overlap function is now dependent on c_0 . Raising this parameter causes the overlap function to be zero for smaller values of $|\delta|$, indicating increased sensitivity to displacement compared to coherent states. Generally, the sensitivity of a coherent state $|\alpha\rangle$ is independent of the specific value of α , which relates to the average photon number by $|\alpha|^2$. Consequently, increasing the average photon number does not enhance the sensitivity of a coherent state to displacements, which is solely limited by the shot noise introduced by vacuum fluctuations [17].

In summary, for the compass state under consideration, sensitivity to displacement appears to be associated with the macroscopic parameter c_0 ; as c_0 grows, it increases both sensitivity and the average photon number in the state. This suggests that a compass state with a larger average photon number can have greater susceptibility to displacement. Furthermore, in this example, the sensitivity to displacement is anisotropically amplified, as illustrated by the tile-like structures around the origin in Fig. 3. Our main focus is on the four-headed kitten state, which is shown in Fig. 1(a). It is evidenced that this particular case is devoid of negative amplitudes, and the dimensions of its phase-space feature are also comparable to those of the coherent states given that sub-Planck structures are absent in this case, and our multiphoton illustrations are specifically devoted to this case, and we

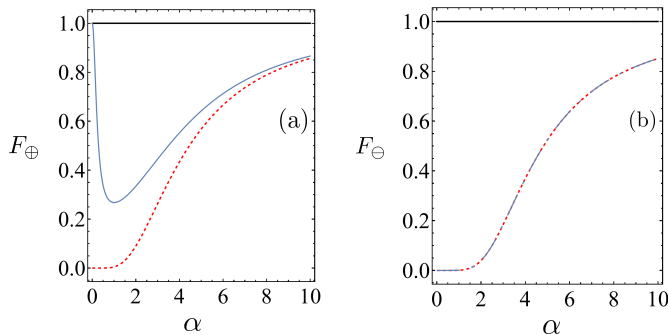


FIG. 4. The overlap between the coherent and deformed versions: (a) For the SA version of the coherent state, the red dotted line represents $r = 4$, $q = 0$, and the blue solid line represents $r = 4$, $q = 4$; (b) For the AS version of the coherent state, the red dotted line corresponds to $r = 4$, $q = 0$, and the blue solid line represents $r = 4$, $q = 4$. The horizontal black solid lines indicate the case where $r = 0$ and $q = 0$, representing the overlap between two ordinary coherent states.

will demonstrate how these photon operations will alter its phase-space characteristics by keeping c_0 a constant.

III. REFINED PHASE-SPACE DENSITIES

Multiphoton operations have been used both theoretically and experimentally to enhance the phase-space characteristics of a quantum state. Techniques involving photon addition (or subtraction) to squeezed-vacuum states have been effectively utilized to generate Schrödinger cat states [50–53] and can also produce multi-component cat states [36, 48], highlighting the benefits of multi-photon operations. In our current work, we use photon addition and subtraction operations on quantum states to create innovative nonclassical quantum states. These newly proposed states could potentially align with modern experimental setups, as discussed in [52, 53]. In the following sections, we present the quantum states that are the focus of our study, accompanied by a thorough theoretical investigation. This detailed analysis explores the phase-space characteristics and implications of these quantum states, providing a comprehensive understanding of their characteristics and significance.

A. Deformed coherent states

In this section, we review the basic concepts that lead to our primary quantum states; especially, we discuss the concept of deformed coherent states [54–56]. Deformed coherent states can be generated by applying a sequence of photon addition and subtraction, or vice versa, to a standard coherent state.

Consider the scenario where r photons are first added to a state, followed by the subtraction of q photons. This

sequence appears as subtraction and addition (SA) operations and is denoted for a coherent state as

$$|\oplus\rangle := N_{\oplus}^{-1/2} \hat{a}^q \hat{a}^{\dagger r} |\alpha\rangle, \quad (12)$$

where

$$N_{\oplus} = (-1)^{r+q} \sum_{n=0}^r \Gamma H_{r-n,q} [i\alpha, i\alpha^*] \times H_{r-n,q} [i\alpha^*, i\alpha] \quad \text{with } \Gamma := \frac{(-1)^n (r!)^2}{n! [(r-n)!]^2} \quad (13)$$

represents the normalization coefficient and $H_{x,y}$ denotes the bivariate Hermite polynomial.

In the addition-subtraction (AS) scenario, the process involves first subtracting q photons from a state, followed with the addition of r photons. This sequence of operations for a coherent state can be denoted as

$$|\ominus\rangle := N_{\ominus}^{-1/2} \hat{a}^{\dagger r} \hat{a}^q |\alpha\rangle \quad (14)$$

with

$$N_{\ominus} = |\alpha|^{2q} \sum_{n=0}^r (-1)^n \Gamma |\alpha|^{2(r-n)} \quad (15)$$

denotes the corresponding normalization coefficient.

To illustrate the impact of photon addition and subtraction operations on a coherent state, we calculate the overlap between the coherent state and its SA and AS variants. The overlap between the coherent state $|\alpha\rangle$ and its SA version $|\oplus\rangle$ is denoted as $F_{\oplus}(\alpha) := |\langle \alpha | \oplus \rangle|^2$, while the overlap in the AS case is denoted as $F_{\ominus}(\alpha) := |\langle \alpha | \ominus \rangle|^2$. These overlaps are evaluated numerically and are represented in Fig. 4. This illustrates that both SA and AS situations differ significantly from the coherent in lower α ranges, and as α grows, corresponding SA and AS variants of the coherent state simply transform back to the ordinary coherent state. This comparison is carried out with different amounts of photon addition r and subtraction q , as shown in Fig. 4(a) and Fig. 4(b), respectively. Note that the photon subtraction operation in the AS scenario has no effect, and in this case, it essentially represents the photon-added version of the coherent state. This is shown in Fig. 4(b), where the red dotted line and blue dotted line indicate different q values with the same r values, resulting in the same curve.

The Wigner functions of SA and AS cases can be evaluated using Eq. (1). Compared to their counterparts of ordinary coherent states, these Wigner functions attain non-Gaussian form and may hold negative phase-space attributes for different values of r and q , highlighting their nonclassical nature [54].

First, for the SA example, the relevant Wigner function is derived as

$$W_{|\oplus\rangle}(\beta) = \frac{1}{N_{\oplus}} W_{|\alpha\rangle}(\beta) \sum_{n=0}^r \Gamma H_{r-n,q} [-i\Omega, -i\alpha^*] \times H_{r-n,q} [i\Omega^*, i\alpha], \quad (16)$$

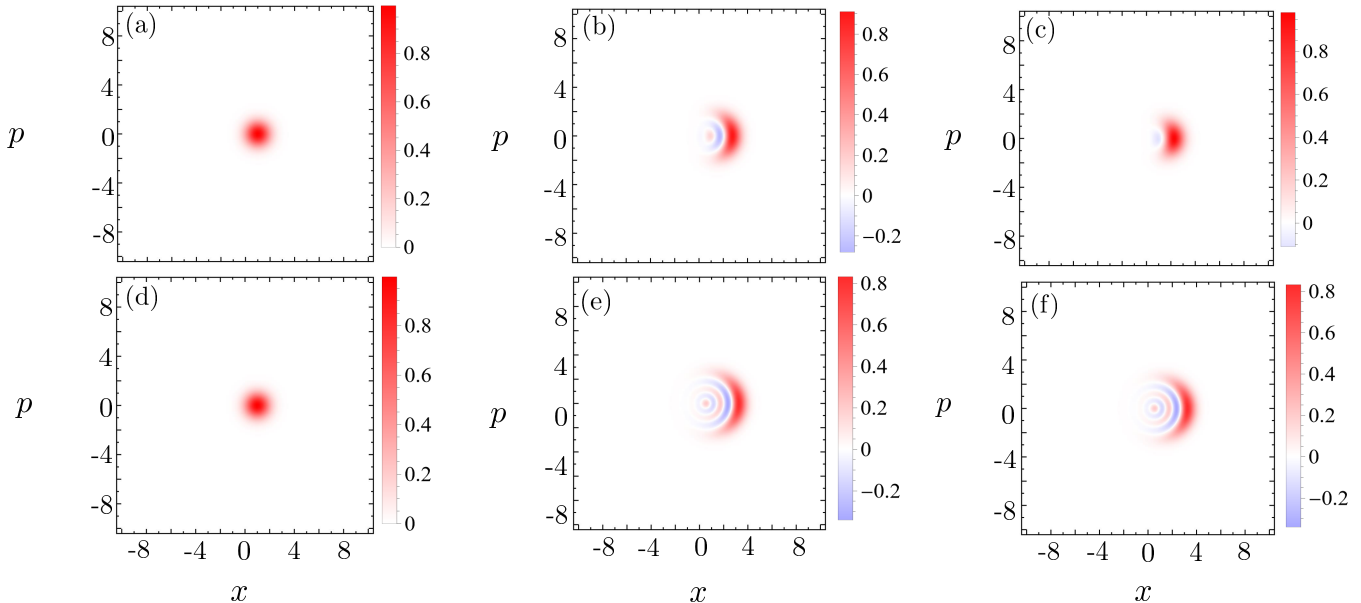


FIG. 5. (a)-(c) represents Wigner distributions of the SA case of a coherent state, and (d)-(f) represents the corresponding AS cases: (a) $r = 0$, $q = 0$; (b) $r = 4$, $q = 2$; (c) $r = 4$, $q = 4$; (d) $r = 0$, $q = 1$; (e) $r = 4$, $q = 2$; and (f) $r = 4$, $q = 4$. In all cases $\alpha = 1/\sqrt{2}$.

where

$$\Omega = 2\beta - \alpha.$$

The non-Gaussian nature of this Wigner function is obvious from the expression, and as it is also evident in Figs. 5(a)-(c) that this Wigner function now acquired negative amplitudes, suggesting the nonclassical nature of this state. Here, note that Fig. 5(a) with $r = 0$ and $q = 0$, presents the case of corresponding ordinary coherent state, but as observed in Figs. 5(b) and 5(c), when r grows, negative regions are amplified, while the q parameter has the opposite impact. Mathematically, the Wigner function for the AS case has an analogous form to that of the SA case.

$$W_{|\Theta\rangle}(\beta) = \frac{(-1)^r}{N_\Theta} W_{|\alpha\rangle}(\beta) \sum_{n=0}^r (-1)^n \Gamma(2\beta - \alpha)^{r-l} \times (\alpha^* - 2\beta^*)^{r-l}. \quad (17)$$

This Wigner function is shown in Figs. 5(d)-(f) with different r and q values, indicating that the corresponding Wigner functions also contain negative amplitudes in the phase space. Note that in this case q has no effect on the state, as shown in Fig. 5(d) with $r = 0$ and $q = 2$ appearing to have the same Wigner function as a coherent state. This is additional evidence that the photon subtraction effect in the indicated AS case is zero, which simply reflects the photon-added case. The photon subtraction from a coherent state leaves the state unchanged is experimentally proved [57]. As illustrated in Fig. 5(e), similar to the SA case, the photon addition

in this case also enhances the negative regions. Furthermore, as observed in Fig. 5(f), with a nonzero value of r , the parameter q remains ineffective. The effects of r and q on the phase space are more thoroughly discussed for the quantum states presented in the following sections.

To emphasize that, as presented in Fig. 5, it is clear that both SA and AS cases presented above are non-Gaussian, and the negativity in their Wigner functions confirms their nonclassical nature, which lacks in the original coherent states. The addition and subtraction (or subtraction and addition) of an equal number of photons from a quantum state can result in two different quantum states. This is confirmed here by two AS and SA cases of coherent states with equivalent photon operations resulting in distinct quantum states, as shown by their Wigner function graphs, and can also be confirmed by the non-commutativity of the bosonic operators \hat{a}^\dagger and \hat{a} .

B. Fluctuations in photon numbers

The photon addition and subtraction operations, as examined in our case, are anticipated to affect the photon number distribution (PND) of our quantum states. For example, in the compass state, the sizes of sub-Planck structures, phase-space sensitivity, and PND are all proportional to the macroscopic parameter. We now illustrate the effects of multi-photon operations on the photon statistics of resulting deformed coherent states. To investigate the PND in these SA and AS scenarios of the coherent state, we use the mathematical expression for PND

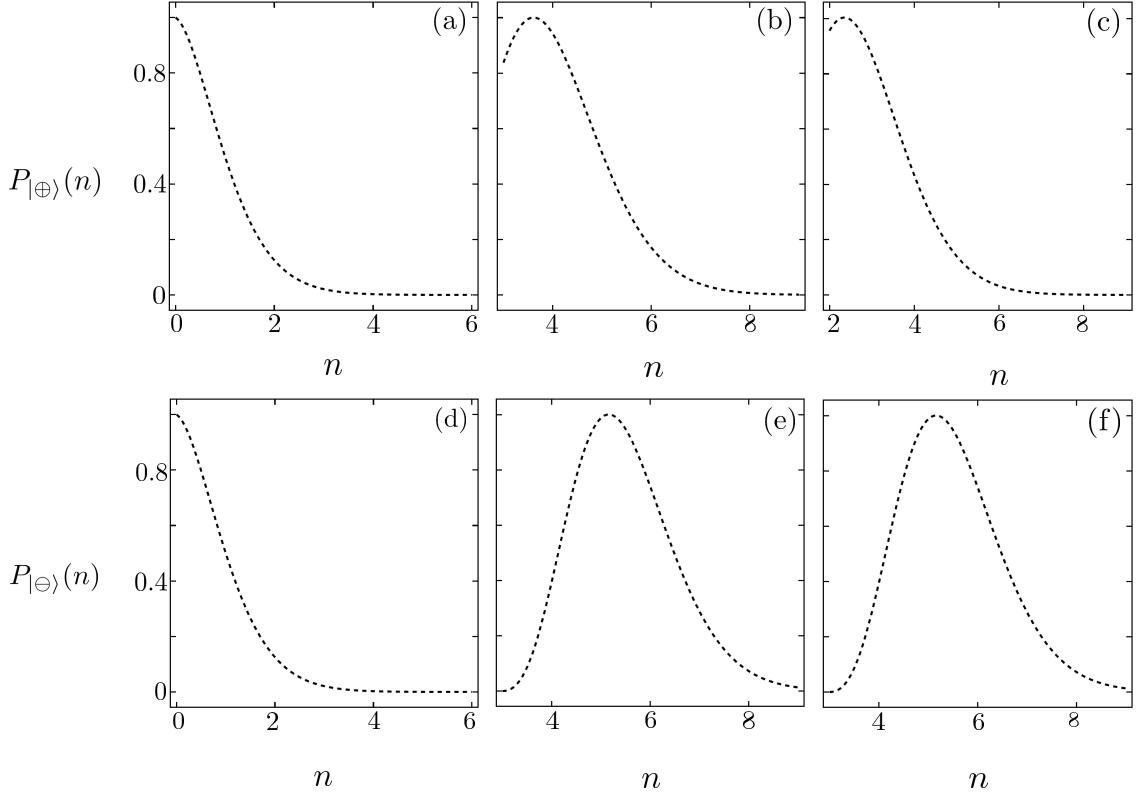


FIG. 6. PND for SA and AS cases are represented by $P_{|\oplus\rangle}(n)$ and $P_{|\ominus\rangle}(n)$, respectively. (a) $r = 0, q = 0$; (b) $r = 4, q = 2$; (c) $r = 4, q = 4$; (d) $r = 0, q = 2$; (e) $r = 4, q = 2$; and (f) $r = 4, q = 4$. We use $\alpha = 1/\sqrt{2}$ in all cases, and distributions are normalized to unity.

of a quantum state $|\psi\rangle$, denoted as $P_{|\psi\rangle}(n) := |\langle n|\psi\rangle|^2$, where $|n\rangle$ represents the Fock state [7].

The photon number distributions for the SA and AS cases, denoted as $P_{|\oplus\rangle}(n)$ and $P_{|\ominus\rangle}(n)$, are evaluated as follows:

$$P_{|\oplus\rangle}(n) = \frac{N_{\oplus}[(q+n)!]^2 \kappa}{n![(q+n-r)!]^2} \text{ and } P_{|\ominus\rangle}(n) = \frac{N_{\ominus} n! \kappa}{[(n-r)!]^2} \quad (18)$$

with

$$\kappa := |\alpha|^{2(q-r+n)} e^{-|\alpha|^2}. \quad (19)$$

Let us now analyze these distributions. Here, Figs. 6(a)-(c) show the PND for the SA case of the coherent state for different situations based on the varying amount of added and subtracted photons. As depicted in Fig. 6(a), PND with $r = 0$ and $q = 0$ exhibits a Poissonian distribution, which obviously corresponds to a coherent state. In Fig. 6(b), when $r = 4$ photons are added and set $q = 0$, the Poissonian distribution shifts to higher values of n , with the peak now occurring at a larger mean photon number. In Fig. 6(c), the Poissonian distribution shifts to lower values of n , as with an increment in the subtracting photons to $q = 4$, and the number of added photons is kept at $r = 4$ as in the prior instance. These

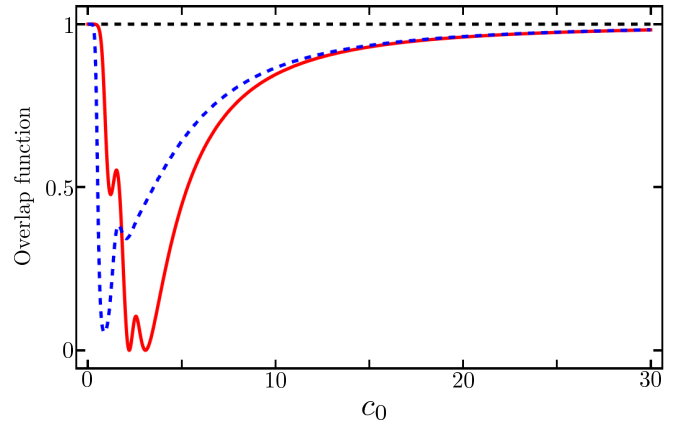


FIG. 7. The overlap function $|F_{\square}(c_0)|^2$ is represented as a blue dashed curve and $|F_{\blacksquare}(c_0)|^2$ as a red solid line, with $r = 4$ and $q = 4$. The horizontal black dashed line depicts the case where $r = 0$ and $q = 0$; consequently, the overlap is simply between two compass states.

cases reflects that in the SA examples, a higher r corresponds to a higher average photon number, whereas a higher q corresponds to a lower average photon number in the resultant state.

The PND for AS case is shown in Figs. 6(d)-(f) with a few r and q values. As illustrated in Fig. 6(d), for $q = 2$ and $r = 0$, the statistics of PND stay constant, showing that raising the number of subtracted photons has no influence on the average photon number of the states when applied directly to a coherent state. As observed in Fig. 6(e), increasing the number of added photons while maintaining the number of subtracted photons constant, that is, with $r = 4$ and $q = 2$, drives the Poissonian distribution to a larger n . In Fig. 6(f), the number of subtracted photons is increased to $q = 4$ without changing r , and it is observed that subtracting photons from a coherent state has no influence on the related PND. This is an additional confirmation of how photon subtraction operations keeps PND of this case invariant. Hence, photon addition in both the SA and AS situations increases the average photon number in the subsequent states; however, the AS case maintains the distribution at higher mean photon values, implying that this situation has higher average photon numbers than the SA case.

C. Impact of multiphoton operations

In §III A, we noticed that the SA and AS variants of a standard coherent state exhibit fascinating phase-space properties that surpass those of the original coherent states. It is observed that the sequence in which photon operations are applied significantly affects the outcome, resulting in two distinct quantum states with different phase-space characteristics. We now extended this basic notion to the main quantum states of the present work.

First, for our SA scenario, r photons are added to the kitten state $|\diamond\rangle$ as given in Eq. (5), followed by the subtraction of q photons. In the AS scenario, q photons are first subtracted from the compass state, and then r photons are added. These photon operations on the kitten state produce new quantum states with distinct phase-space characteristics.

The resulting SA case is denoted as $|\square\rangle$ and mathematically described as:

$$|\square\rangle := N_{\square}^{-1/2} \hat{a}^q \hat{a}^{\dagger r} \sum_{i=1}^4 |\alpha_i\rangle \quad (20)$$

with

$$N_{\square} = (-1)^{r+q} \sum_{i,j=1}^4 \sum_{n=0}^r \Gamma G_{\alpha_i, \alpha_j} e^{\alpha_i^* \alpha_j} H_{r-n, q} [i\alpha_j, i\alpha_i^*] \times H_{r-n, q} [i\alpha_i^*, i\alpha_j] \quad (21)$$

denotes the normalization coefficient.

In the same way, the AS situation, denoted as $|\blacksquare\rangle$, is represented as follows:

$$|\blacksquare\rangle := N_{\blacksquare}^{-1/2} \hat{a}^{\dagger r} \hat{a}^q \sum_{i=1}^4 |\alpha_i\rangle, \quad (22)$$

where

$$N_{\blacksquare} = \sum_{i,j=1}^4 \sum_{n=0}^r (-1)^n \Gamma G_{\alpha_i, \alpha_j} e^{\alpha_i^* \alpha_j} (\alpha_i \alpha_j)^q (\alpha_j)^{r-n} (\alpha_i^*)^{r-n} \quad (23)$$

represents the normalization factor for this case. When photon subtraction is combined with a photon addition operator, the effect of the parameter q is highly apparent, as we will show later in the following discussion.

We now compare the original compass state with the proposed variants by assessing their overlap. This overlap indicates how distinct the proposed states are from the original compass state. The overlap between our SA case and the compass state is represented by $F_{\square}(c_0) := \langle \square | \diamond \rangle$ and is calculated as

$$F_{\square}(c_0) = (-i)^{r+q} [N_{\square} N_{\diamond}]^{-1/2} \sum_{i,j=1}^4 F_{|\square_i\rangle \langle \square_j|} \quad (24)$$

with

$$F_{|\square_i\rangle \langle \square_j|} := G_{\alpha_i, \alpha_j} e^{\alpha_i^* \alpha_j} H_{r, q} [i\alpha_i^*, i\alpha_j], \quad (25)$$

and is depicted with a blue dashed line in Fig. 7.

Now, we provide the overlap between AS and compass state, which is denoted as $F_{\blacksquare}(c_0) := \langle \blacksquare | \diamond \rangle$. This overlap reads

$$F_{\blacksquare}(c_0) = [N_{\blacksquare} N_{\diamond}]^{-1/2} \sum_{i,j=1}^4 F_{|\blacksquare_i\rangle \langle \blacksquare_j|} \quad (26)$$

with

$$F_{|\blacksquare_i\rangle \langle \blacksquare_j|} := G_{\alpha_i, \alpha_j} e^{\alpha_i^* \alpha_j} (\alpha_i^*)^q (\alpha_j)^r, \quad (27)$$

and is plotted with a red solid line in Fig. 7.

In Fig. 7, the black dotted line represents the overlap between two same compass states, and recalling that the parameter c_0 measures the distance from the origin of the phase space, as discussed in §II B, this parameter has a strong impact on the characteristics of the original state, that is, the existence of the sub-Planck structures, and enhanced sensitivity is associated with higher c_0 values. For example, the scenario represented in Fig. 1(a) for comparatively smaller values of c_0 does not have the capacity to exhibit these traits, and this particular case is named as a four-headed kitten state in the present work.

Note that in our plots, we only investigate the overlaps for the certain situation when $r = q = 4$, because it is understood here that for other higher values of r and q , our proposed states keep the difference than the compass state provided that c_0 is smaller, as depicted here; simply, this result is meaningful for other settings of r and q . In these plots, it is clear that greater c_0 values push the blue dotted and red solid lines closer to the horizontal black dotted line, implying that the SA and AS cases revired to the original compass state. In our work, we set $c_0 = 1$ and

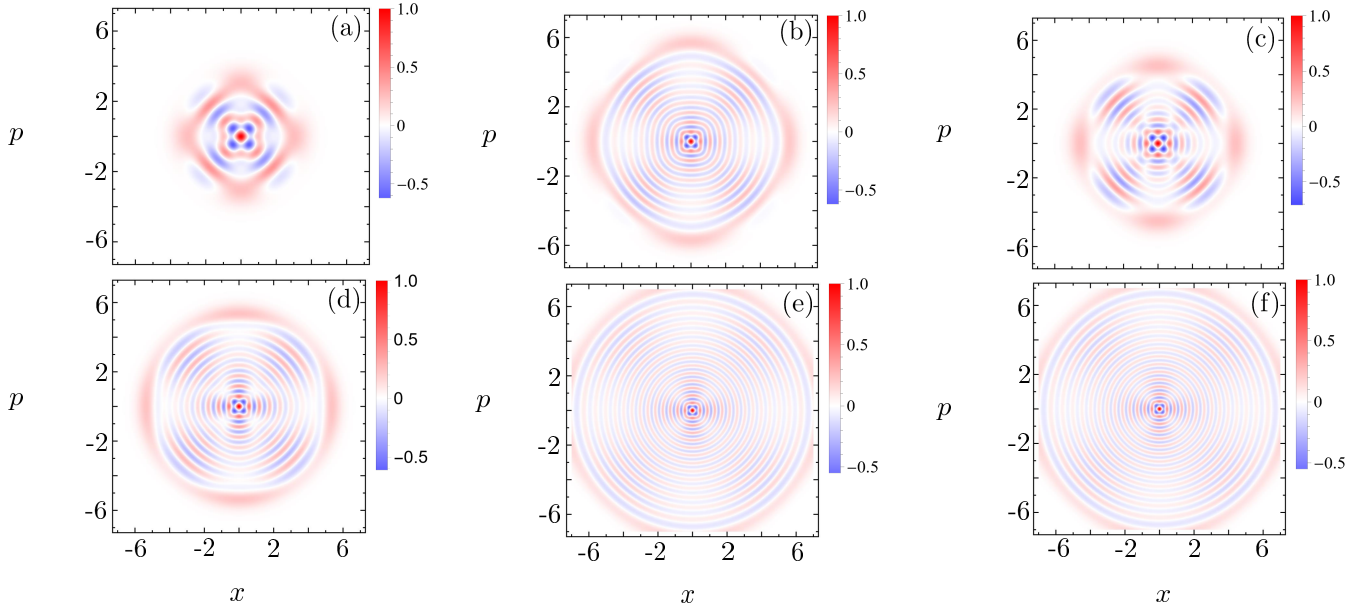


FIG. 8. (a)-(c) show the Wigner function of the SA case of the four-headed kitten state, and (d)-(f) show the analogous AS cases. (a) $r = 12$, $q = 12$, (b) $r = 24$, $q = 12$, (c) $r = 24$, $q = 20$, (d) $r = 12$, $q = 12$, (e) $r = 24$, $q = 12$, and (f) $r = 24$, $q = 20$. In all cases, $c_0 = 1$.

investigate the corresponding phase-space characteristics of the four-headed cat state using multiple options of photon addition and subtraction operations. Here, we simply refer to these consequent states as SA and AS cases of this kitten state. Here, note that our AS case is the eigenstate of the operator \hat{a}^4 , i.e., $\hat{a}^4 |\blacksquare\rangle = |\diamond\rangle$. This shows that choosing the parameter q as a multiple of 4 ($q = 4k$ with $k \in \mathbb{N}^+$) corresponds to a photon-added version of the compass state. When $p = 0$, this reduces to the compass state $|\diamond\rangle$ itself.

D. Unique phase-space features

In the previous section, we have introduced the SA and AS cases of our interest, each producing distinct quantum states. In these instances, photon addition and subtraction processes appeared to have a main impact on their phase-space characteristics, and in this section, we particularly employ the Wigner function to investigate the corresponding phase space of these quantum states. To obtain the Wigner function for each case, Eq. (1) is employed, and we denote $W_{|\square\rangle}(\beta)$ and $W_{|\blacksquare\rangle}(\beta)$ as the corresponding Wigner functions of SA and AS cases of the kitten state, respectively.

Let us now examine the Wigner distributions for each scenario. For the SA case of our four-headed kitten state introduced in Eq. (20), the Wigner distribution is calculated as follows:

$$W_{|\square\rangle}(\beta) = \frac{1}{N_{\square}} \sum_{i,j=1}^4 W_{|\square_i\rangle\langle\square_j|}(\beta), \quad (28)$$

where

$$W_{|\square_i\rangle\langle\square_j|}(\beta) := W_{|\alpha_i\rangle\langle\alpha_j|}(\beta) \sum_{n=0}^r \Gamma H_{r-n,q} [i\Omega_j^*, i\alpha_i] \times H_{r-n,q} [-i\Omega_i, -i\alpha_j^*] \quad (29)$$

with

$$\Omega_{\mu} := 2\beta - \alpha_{\mu}. \quad (30)$$

In the same way, for the AS situation depicted in Eq. (22), we have

$$W_{|\blacksquare\rangle}(\beta) = \frac{(-1)^r}{N_{\blacksquare}} \sum_{i,j=1}^4 W_{|\blacksquare_i\rangle\langle\blacksquare_j|}(\beta), \quad (31)$$

where

$$W_{|\blacksquare_i\rangle\langle\blacksquare_j|}(\beta) := (\alpha_i \alpha_j^*)^q W_{|\alpha_i\rangle\langle\alpha_j|}(\beta) \sum_{n=0}^r (-1)^n \Gamma (2\beta - \alpha_i)^{r-n} \times (\alpha_j - 2\beta^*)^{r-n}. \quad (32)$$

The relevant Wigner functions are presented in Figs. 8, with Fig. 9 illustrating the zoom in of the central phase-space features of each case, where for both figures the cases labelled with (a)-(c) exhibit the SA, while (d)-(f) provides equivalent AS cases of the kitten state. With specific selections of the parameters r and q , Fig. 10 offers a further illustration of the Wigner function of corresponding AS scenarios.

It is readily apparent that our SA and AS instances achieve substantially distinct phase-space characteristics

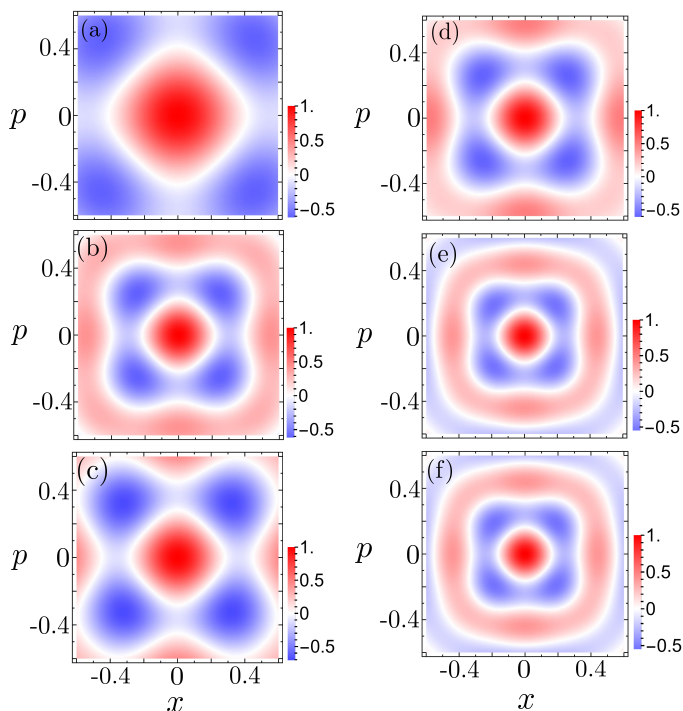


FIG. 9. Zoom in on the central phase-space structures of the cases shown in Fig. 8. The cases on the left are SA, whereas the cases on the right are AS. (a) $r = 12$, $q = 12$; (b) $r = 24$, $q = 12$; (c) $r = 24$, $q = 20$; (d) $r = 12$, $q = 12$; (e) $r = 24$, $q = 12$; (f) $r = 24$, $q = 20$. In each example, $c_0 = 1$.

as compared to the four-headed kitten state. Interestingly, a central sub-Planck structure is identified in each of the cases outlined. We focus on the significance of the sub-Planck structure in these states and examine this particular phase-space feature in detail.

Photon addition and subtraction appeared to have significant effects on the Wigner distribution of the corresponding states. Note that the original four-headed kitten state, represented in Fig. 1(a) with $c_0 = 1$, does not exhibit a sub-Planck structure. This implies that the appearance of the sub-Planck structures in our cases is attributed to the photon operations involved. Specifically, it is observed that as the parameter r , which represents the number of added photons, increases, the size of the sub-Planck structure reduces uniformly in both the SA and AS cases. This is evident by comparing the scenarios presented in Figs. 9(a) and 9(b) for the SA case, and then Figs. 9(d) and 9(e) are for corresponding AS cases, where increasing r with constant q , clearly depicts this impact. Furthermore, increasing the number of photon subtractions q increases the size of the sub-Planck structure in the SA case, as observed by comparing cases depicted in Figs. 8(b) and 8(c), while it has no effect in the AS case, as shown in Figs. 8(e) and 8(f). Note that all the examples of AS described in Figs. 8 and 9 correspond to the merely photon-added case of the compass state, as for these situations q are the multiple of 4, where the

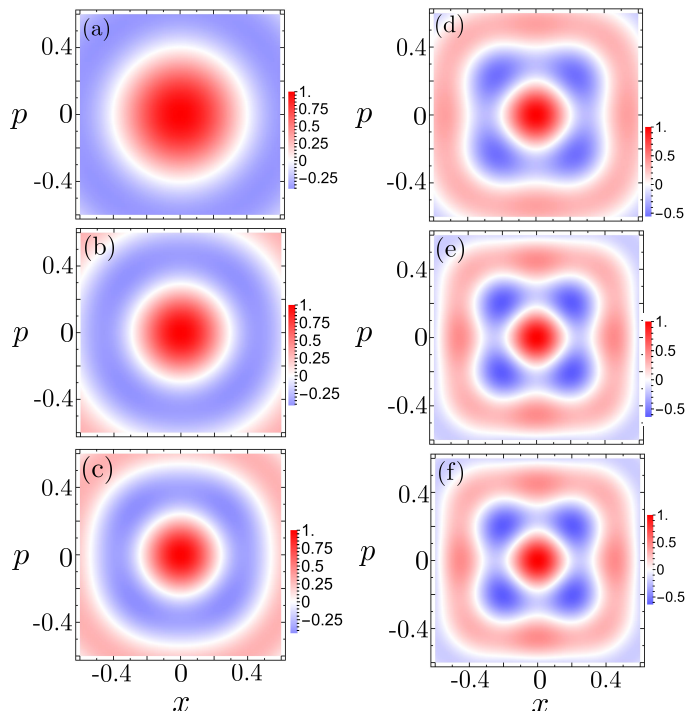


FIG. 10. The zoom in on the center phase-space structures of the four-headed kitten state with multiple parameter r and q values. (a) $r = 1$, $q = 1$; (b) $r = 5$, $q = 5$; (c) $r = 9$, $q = 9$; (d) $r = 16$, $q = 10$; (e) $r = 22$, $q = 10$; (f) $r = 22$, $q = 18$. For all cases, $c_0 = 1$.

corresponding four-headed kitten state is the eigenstate of the operator \hat{a}^4 .

We find that photon addition generally reduces the size of sub-Planck structures in both SA and AS scenarios, while photon subtraction increases their size in the SA case but has no effect on their size in the AS case. To further illustrate this for the AS case, we examine situations where the number of photon subtractions is not a multiple of 4, as shown in Fig. 10. Increasing the photon addition to the state as previously noted also reduces the size of the sub-Planck structures for this specific illustration (Figs. 10(d) and 10(e)), while as expected, varying the photon subtraction in these cases has no impact on the size of the sub-Planck structures (Figs. 10(e) and 10(f)), but in some specific instances, photon subtraction slightly enhances the isotropy of the sub-Planck structures. For example, an enhancement in the isotropy of the central sub-Planck structures of these cases is clearly evident in Figs. 10(a) to 10(c), as demonstrated by the circular structure around the origin. This indicates that, for these scenarios, the sub-Planck structure is uniformly constrained in all directions of the phase space.

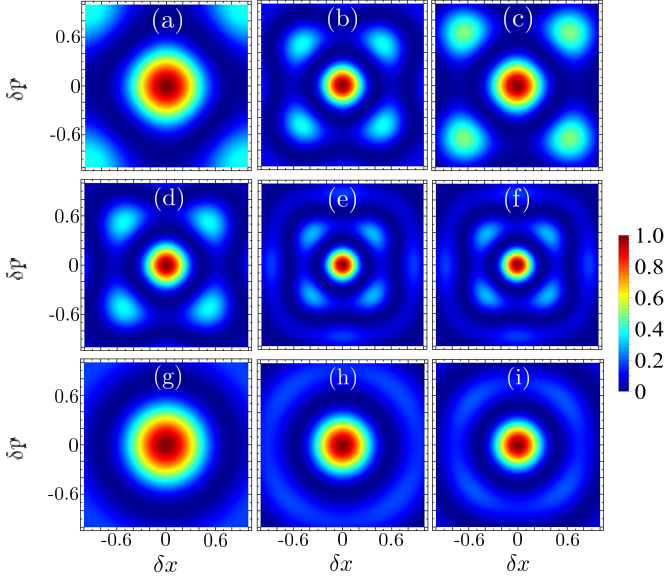


FIG. 11. Overlap between a state and its slightly translated version with (a)-(c) depict SA examples, whereas (d)-(i) exhibit comparable AS cases: (a) $r = 12$, $q = 12$, (b) $r = 24$, $q = 12$, (c) $r = 24$, $q = 20$, (d) $r = 12$, $q = 12$, (e) $r = 24$, $q = 12$, (f) $r = 24$, $q = 20$, (g) $r = q = 1$, (h) $r = q = 5$, and (i) $r = q = 9$. In all situations, we set $c_0 = 1$ and normalize the intensity plots to unity.

IV. ENHANCEMENT IN SENSITIVITY

Sensitivity and its relationship to the phase-space characteristics of a quantum state are thoroughly discussed in the §II A. This concept is then applied to the compass state in the §II B, where it is demonstrated that the presence of sub-Planck structures in those states significantly have enhanced their sensitivity to displacement and that optimizing controlling parameters may further enhance this sensitivity far better than the standard quantum limit. In §III D, we thoroughly examined the phase space of the proposed SA and AS cases, confirming the presence of sub-Planck structures in their phase spaces. We now examine how these sub-Planck structures have impact on the sensitivity to phase-space displacement, which is analyzed by assessing the sensitivities using Eq. (3).

First, for the SA scenario, we denote the associated sensitivity as $S_{|\square\rangle}(\delta)$, and is calculated as

$$S_{|\square\rangle}(\delta) = \left| \sum_{i,j=1}^4 O_{|\square_i\rangle\langle\square_j|}(\delta) \right|^2 \quad (33)$$

with

$$O_{|\square_i\rangle\langle\square_j|}(\delta) := G_{\alpha_i, \alpha_j} \Lambda \sum_{n=0}^r (-1)^n \Gamma H_{r-n, q} [i(\alpha_i^* - \delta^*), i\alpha_j] \times H_{r-n, q} [-i(\alpha_j + \delta), -i\alpha_i^*] \quad (34)$$

and

$$\Lambda := \exp \left[-\alpha_j \delta^* - \frac{|\delta|^2}{2} + \alpha_i^* \alpha_j + \alpha_i^* \delta \right]. \quad (35)$$

In the AS situation, the sensitivity $S_{|\blacksquare\rangle}(\delta)$ is found as

$$S_{|\blacksquare\rangle}(\delta) = \left| \sum_{i,j=1}^4 O_{|\blacksquare_i\rangle\langle\blacksquare_j|}(\delta) \right|^2, \quad (36)$$

where

$$O_{|\blacksquare_i\rangle\langle\blacksquare_j|}(\delta) := (\alpha_i \alpha_j^*)^q G_{\alpha_i, \alpha_j} \Lambda \sum_{n=0}^r (-1)^n \Gamma (\alpha_i^* - \delta^*)^{r-n} \times (\alpha_j + \delta)^{r-n}. \quad (37)$$

The corresponding sensitivities $S_{|\square\rangle}(\delta)$ and $S_{|\blacksquare\rangle}(\delta)$ with $\delta := (\delta x + i\delta p)/\sqrt{2}$ are shown in Fig. 11.

Let us now examine the SA cases presented in the Figs. 11(a)-(c) belong to the SA situation, where it is evident that the overlap is zero for values $|\delta| < 1$ (less than a coherent state) along arbitrary directions in phase space. This indicates that the sensitivity to displacement in this scenario surpasses the standard limit. The enhancement in sensitivity becomes more pronounced as the parameter r , which represents the number of added photons to the kitten state, increases. As shown in Figs. 11(a) and 11(b), this effect becomes clearly noticeable with a higher number of added photons. Specifically, the central structure is significantly reduced when the number of added photons increases from $r = 12$ to $r = 24$ with the number of subtracted photons, $q = 12$, remains constant in this situation. Furthermore, the impact of increasing the number of eliminated photons from $q = 12$ to $q = 20$ is illustrated in the Figs. 11(b) and 11(c), where an enlargement in the central structure occurs, indicating that a higher value $|\delta|$ relative to the earlier case represented in Fig. 11(b) is needed to make the overlap zero. This suggests that the sensitivity to displacement in this circumstance decreases with an increment in q ; hence, contrary to the parameter r , increasing the number of subtracted photons reduces sensitivity in the SA scenario.

In the AS scenario, as depicted in Figs. 11(d)-(f), comparable to the SA example, an improved sensitivity to phase space displacements δ is observed. The values $|\delta| < 1$ can render the $S_{|\blacksquare\rangle}(\delta)$ zero as observable by the central structure. Similar to the SA example, this amplification becomes more noticeable as r increases, as illustrated in the instances depicted in Figs. 11(d) and 11(e), where an increment in the r as shown in Fig. 11(e) has reduced the central structure corresponding to the overlap function, meaning that now a smaller value of $|\delta|$ is required to make the overlap zero compared to the case shown in Fig. 11(d). Furthermore, we observe that in Fig. 11(e) and Fig. 11(f), the photon subtraction q also does not affect the sensitivity enhancement as depreciated; in Fig. 11(f), raising q results in the same overlap

as its preceding instance. However, the photon subtraction q may have an effect on the isotropic nature of the sensitivity, as optimal parameter selections may produce isotropic regions, such as the circle-type regions centered at the origin observed in Figs. 11(g) to 11(i) show that in the AS scenario, sensitivity is consistently increased in all directions, making these instances better compared to their counter parts of SA and compass states.

V. OUTLOOK

We now provide a brief discussion on our results with their summarized physical consequences. This comprehensive discussion strives to integrate our findings into current understanding, providing a detailed picture of their effects and contributions to the field.

A four-headed kitten state is considered a main example in our study, which represents a smaller version of a compass state [13], and our investigations and discussion are centered around this state, which serves as the foundation for our exploration and examination. The compass state exhibits fascinating sub-Planck scale structures and enhanced sensitivity. However, these characteristics are lost when transitioning to a kitten state [52], which is essentially a smaller version of the cat state, as the one we presented in Fig. 1(a). This transition occurs when the macroscopic parameter is reduced, resulting in a transformation from a cat state to a kitten state. Specifically, a bigger compass state exhibits pronounced sub-Planck features, indicating more finer quantum characteristics at scales lower than the Planck length, as discussed in §II B and then depicted in Fig. 1. Note that the mean photon number in bigger catlike states is higher [24], indicating enhanced total photon content and intensity. This comparison demonstrates the significant differences in quantum behavior and measurement precision between the larger compass and kitten states, as observed in Fig. 3.

Photon addition and subtraction operations on squeezed-vacuum states are extremely useful approaches for creating larger cat states [50–53]. These methods have also been demonstrated experimentally and provide an effective way to generate cat states of larger amplitude [52, 53]. In this study, we utilized the kitten version of the compass state and applied photon addition and subtraction operations with different order and magnitudes to construct our novel variants, as presented in Figs. 8, 9 and 10. We then investigated the phase-space characteristics of these variants to gain insights into their quantum properties. The kitten version of the compass state, as shown in Fig. 1(a), which does not possess sub-Planckness, is now transformed into the states holding sub-Planck structures and demonstrating an enhanced sensitivity, implying the effectiveness of these multi-photon processes, as evident in Fig. 11.

When the number of photons added increases, nonclassical features contained by these states are improved, but

increasing photon subtraction destroys nonclassical sub-Planck structures in phase space. Note that this only occurs for our SA case; otherwise, when photon subtraction is applied to a state directly (AS cases), the phase space nearly remains unchanged [see Fig. 5], and the size of the sub-Planck structures of the AS cases stays constant over the variation of the photon subtraction operations. Furthermore, photon addition raises the average photon count in the states, whereas photon subtraction maintains the photon statistics invariant. This demonstrates that the sequence of photon addition and subtraction operations in our case has a direct effect on the amount of quanta present in the states, which may be useful in maintaining the photon number in our states rather efficiently.

Our quantum states exhibit comparable phase-space attributes as the compass state when there is a large number of the photon addition of the photons is applied to the four-headed kitten state, and the role of the photon subtraction in our instances is also interesting as in some cases it slightly enhances the isotropy of these features. Distinct phase-space characteristics between our SA and AS examples are highlighted, namely that AS cases have smaller sub-Planck structures and so achieve higher sensitivity when compared to their SA counterparts. Our investigation implies that variants of the four-headed kitten state we provided are an appropriate substitute for compass states and may perform better compared to the compass state under optimum conditions.

VI. CONCLUSION

We introduced alternative versions of the compass state, which are obtained by adding (and subtracting) an immense number of photons to a four-headed kitten state, with the option that the order in which these photons are applied to the state also changes and the non-commutativity of the bosonic operators results in two different quantum states with distinct phase-space features. Our outcomes revealed that the multiphoton operations we performed on the four-headed kitten state are quite effective and that these operations have transformed this multicomponent kitten state to other forms of states, which are richer in their nonclassical phase-space features and also exhibit sub-Planck structures. This investigation is relevant to previous experimental studies [52, 53], which demonstrated that photon operations are an effective means of enhancing the phase-space characteristics of quantum states, thereby supporting our findings.

The presence of crucial sub-Planck structures in the present investigation is influenced by the number of photons added or subtracted. Adding photons helps preserve these structures in both scenarios we explored, while subtracting photons typically disrupts them when photon addition is followed by photon subtraction. However, photon subtraction alone has no effect on the sub-Planck structures if applied before photon addition, and in this

case (subtraction then addition), specific choices of photon subtraction operations may lead to isotropic versions of sub-Planck structures. These results directly apply to the sensitivity of these states as well. The sensitivity to displacement of the quantum states we proposed exceeds the standard limits, and this enhancement is also controlled by multiphoton operations. Specifically, increasing photon addition enhances sensitivity, while photon subtraction reduces it, in the sequence where photon addition is followed by subtraction. However, in the converse case of photon operations, the sensitivity to displacement remains unchanged over the variation of the photon subtraction, although, interestingly, for this case, improvement in the isotropy of sensitivity is observed for certain photon subtraction choices. The induction of sub-Planck structures in our indicated situations connects them to recent techniques for the devel-

opment of nonclassical traits in quantum states [50–53]. Perhaps these techniques may also be applied in the development of the quantum states we provided. Future research may inquire how to create our proposed quantum states, which will require a novel and thorough investigation to develop new techniques for their generation. This endeavor may involve formulating innovative strategies and methodologies specifically designed to produce these advanced quantum states.

ACKNOWLEDGMENT

This work is supported by the Natural Science Foundation of Jiangsu Province (Grant No. BK20231320) and the National Natural Science Foundation of China (Grant No. 12174157).

-
- [1] E. Schrödinger, Der stetige Übergang von der mikro- zur makromechanik, *Sci. Nat.* **14**, 664 (1926).
- [2] P. W. Milonni and M. M. Nieto, Coherent states, in *Compendium of Quantum Physics*, (Springer, Berlin, Heidelberg, 2009).
- [3] R. J. Glauber, Coherent and incoherent states of the radiation field, *Phys. Rev.* **131**, 2766 (1963).
- [4] C. Gerry and P. Knight, *Introductory Quantum Optics* (Cambridge University Press, England, Cambridge, 2005).
- [5] V. Bužek and P. L. Knight, *Quantum Interference, Superposition States of Light and Nonclassical Effects*, Prog. Opt., Vol. 34 (Elsevier, Amsterdam, 1995) p. 1.
- [6] E. Wigner, On the quantum correction for thermodynamic equilibrium, *Phys. Rev.* **40**, 749 (1932).
- [7] W. P. Schleich, *Quantum Optics in Phase Space* (Wiley-VCH, Weinheim, 2001).
- [8] J. Joo, W. J. Munro, and T. P. Spiller, Quantum metrology with entangled coherent states, *Phys. Rev. Lett.* **107**, 083601 (2011).
- [9] P. Walther, J.-W. Pan, M. Aspelmeyer, R. Ursin, S. Gasparoni, and A. Zeilinger, De Broglie wavelength of a non-local four-photon state, *Nature* **429**, 158 (2004).
- [10] M. W. Mitchell, J. S. Lundeen, and A. M. Steinberg, Super-resolving phase measurements with a multiphoton entangled state, *Nature* **429**, 161 (2004).
- [11] K. Johnson, J. Wong-Campos, B. Neyenhuis, J. Mizrahi, and C. Monroe, Ultrafast creation of large Schrödinger cat states of an atom, *Nat. Commun.* **8**, 697 (2017).
- [12] A. Facon, E.-K. Dietsche, D. Grosso, S. Haroche, J.-M. Raimond, M. Brune, and S. Gleyzes, A sensitive electrometer based on a Rydberg atom in a Schrödinger-cat state, *Nature* **535**, 262 (2016).
- [13] W. H. Zurek, Sub-Planck structure in phase space and its relevance for quantum decoherence, *Nature* **412**, 712 (2001).
- [14] K. M. R. Audenaert, Comparisons between quantum state distinguishability measures, *Quantum Inf. Comput.* **14**, 31 (2014).
- [15] D. Dieks, Overlap and distinguishability of quantum states, *Phys. Lett. A* **126**, 303 (1988).
- [16] S. L. Braunstein and P. van Loock, Quantum information with continuous variables, *Rev. Mod. Phys.* **77**, 513 (2005).
- [17] C. Navarrete-Benlloch, *An Introduction to the Formalism of Quantum Information with Continuous Variables* (Morgan & Claypool/IOP, Bristol, 2015).
- [18] U. Leonhardt, *Measuring the Quantum State of Light*, Vol. 22 (Cambridge university press, Cambridge, England, 1997).
- [19] H. P. Robertson, The uncertainty principle, *Phys. Rev.* **34**, 163 (1929).
- [20] A. Jordan and M. Srednicki, *Sub-Planck structure, decoherence, and many-body environments* (2001), arXiv:quant-ph/0112139 [quant-ph].
- [21] G. J. Milburn, Quantum and classical Liouville dynamics of the anharmonic oscillator, *Phys. Rev. A* **33**, 674 (1986).
- [22] B. Yurke and D. Stoler, Generating Quantum Mechanical Superpositions of Macroscopically Distinguishable States via Amplitude Dispersion, *Phys. Rev. Lett.* **57**, 13 (1986).
- [23] N. Akhtar, B. C. Sanders, and C. Navarrete-Benlloch, Sub-Planck structures: Analogies between the Heisenberg-Weyl and SU(2) groups, *Phys. Rev. A* **103**, 053711 (2021).
- [24] N. Shukla, N. Akhtar, and B. C. Sanders, Quantum tetrachotomous states: Superposition of four coherent states on a line in phase space, *Phys. Rev. A* **99**, 063813 (2019).
- [25] L. A. Howard, T. J. Weinhold, F. Shahandeh, J. Combes, M. R. Vanner, A. G. White, and M. Ringbauer, Quantum hypercube states, *Phys. Rev. Lett.* **123**, 020402 (2019).
- [26] F. Toscano, D. A. R. Dalvit, L. Davidovich, and W. H. Zurek, Sub-Planck phase-space structures and Heisenberg-limited measurements, *Phys. Rev. A* **73**, 023803 (2006).
- [27] P. Jacquod, I. Adagideli, and C. W. J. Beenakker, Decay of the Loschmidt Echo for Quantum States with Sub-Planck-scale Structures, *Phys. Rev. Lett.* **89**, 154103 (2002).

- [28] D. A. Wisniacki, Short-time decay of the Loschmidt echo, *Phys. Rev. E* **67**, 016205 (2003).
- [29] S. Ghosh, A. Chiruvelli, J. Banerji, and P. K. Panigrahi, Mesoscopic superposition and sub-Planck-scale structure in molecular wave packets, *Phys. Rev. A* **73**, 013411 (2006).
- [30] L. Praxmeyer, P. Wasylczyk, C. Radzewicz, and K. Wódkiewicz, Time-Frequency Domain Analogues of Phase Space Sub-Planck Structures, *Phys. Rev. Lett.* **98**, 063901 (2007).
- [31] J. R. Bhatt, P. K. Panigrahi, and M. Vyas, Entanglement-induced sub-Planck phase-space structures, *Phys. Rev. A* **78**, 034101 (2008).
- [32] M. Stobińska, G. J. Milburn, and K. Wódkiewicz, Wigner function evolution of quantum states in the presence of self-Kerr interaction, *Phys. Rev. A* **78**, 013810 (2008).
- [33] S. Ghosh, U. Roy, C. Genes, and D. Vitali, Sub-Planck-scale structures in a vibrating molecule in the presence of decoherence, *Phys. Rev. A* **79**, 052104 (2009).
- [34] U. Roy, S. Ghosh, P. K. Panigrahi, and D. Vitali, Sub-Planck-scale structures in the Pöschl-teller potential and their sensitivity to perturbations, *Phys. Rev. A* **80**, 052115 (2009).
- [35] N. Akhtar, B. C. Sanders, and G. Xianlong, Sub-Planck phase-space structure and sensitivity for SU(1,1) compass states, *Phys. Rev. A* **106**, 043704 (2022).
- [36] N. Akhtar, J. Wu, J.-X. Peng, W.-M. Liu, and G. Xianlong, Sub-Planck structures and sensitivity of the superposed photon-added or photon-subtracted squeezed-vacuum states, *Phys. Rev. A* **107**, 052614 (2023).
- [37] N. Akhtar, X. Yang, M. Asjad, J.-X. Peng, G. Xianlong, and Y. Chen, Compasslike states in a thermal reservoir and fragility of their nonclassical features, *Phys. Rev. A* **109**, 053718 (2024).
- [38] A. Shukla and B. C. Sanders, Superposing compass states for asymptotic isotropic sub-Planck phase-space sensitivity, *Phys. Rev. A* **108**, 043719 (2023).
- [39] D. A. R. Dalvit, R. L. de Matos Filho, and F. Toscano, Quantum metrology at the Heisenberg limit with ion trap motional compass states, *New J. Phys.* **8**, 276 (2006).
- [40] G. S. Agarwal and P. K. Pathak, Mesoscopic superposition of states with sub-Planck structures in phase space, *Phys. Rev. A* **70**, 053813 (2004).
- [41] P. K. Pathak and G. S. Agarwal, Generation of a superposition of multiple mesoscopic states of radiation in a resonant cavity, *Phys. Rev. A* **71**, 043823 (2005).
- [42] Z. Leghtas, G. Kirchmair, B. Vlastakis, M. H. Devoret, R. J. Schoelkopf, and M. Mirrahimi, Deterministic protocol for mapping a qubit to coherent state superpositions in a cavity, *Phys. Rev. A* **87**, 042315 (2013).
- [43] L. C. G. Govia, E. J. Pritchett, and F. K. Wilhelm, Generating nonclassical states from classical radiation by subtraction measurements, *New J. Phys.* **16**, 045011 (2014).
- [44] S. Choudhury and P. K. Panigrahi, A proposal to generate entangled compass states with sub-planck structure, in *AIP Conference Proceedings*, Vol. 1384 (American Institute of Physics, 2011) pp. 91–96.
- [45] N. Ofek, A. Petrenko, R. Heeres, P. Reinhold, Z. Leghtas, B. Vlastakis, Y. Liu, L. Frunzio, S. M. Girvin, L. Jiang, M. Mirrahimi, M. H. Devoret, and R. J. Schoelkopf, Extending the lifetime of a quantum bit with error correction in superconducting circuits, *Nature* **536**, 441 (2016).
- [46] B. Vlastakis, G. Kirchmair, Z. Leghtas, S. E. Nigg, L. Frunzio, S. M. Girvin, M. Mirrahimi, M. H. Devoret, and R. J. Schoelkopf, Deterministically encoding quantum information using 100-photon Schrödinger cat states, *Science* **342**, 607 (2013).
- [47] L. Praxmeyer, C.-C. Chen, P. Yang, S. D. Yang, and R. K. Lee, Direct measurement of time-frequency analogs of sub-Planck structures, *Phys. Rev. A* **93**, 053835 (2016).
- [48] G. B. Lemos, R. M. Gomes, S. P. Walborn, P. H. S. Ribeiro, and F. Toscano, Experimental observation of quantum chaos in a beam of light, *Nat. Commun.* **3**, 2041 (2012).
- [49] J. Wenger, R. Tualle-Brouri, and P. Grangier, Non-Gaussian statistics from individual pulses of squeezed light, *Phys. Rev. Lett.* **92**, 153601 (2004).
- [50] M. Dakna, T. Anhut, T. Opatrný, L. Knöll, and D.-G. Welsch, Generating Schrödinger-cat-like states by means of conditional measurements on a beam splitter, *Phys. Rev. A* **55**, 3184 (1997).
- [51] X.-B. Tang, F. Gao, Y.-X. Wang, J.-G. Wu, and F. Shuang, Non-Gaussian features from excited squeezed vacuum state, *Opt. Commun.* **345**, 86 (2015).
- [52] A. Ourjoumtsev, R. Tualle-Brouri, J. Laurat, and P. Grangier, Generating optical Schrödinger kittens for quantum information processing, *Science* **312**, 83 (2006).
- [53] J. S. Neergaard-Nielsen, B. M. Nielsen, C. Hettich, K. Mølmer, and E. S. Polzik, Generation of a superposition of odd photon number states for quantum information networks, *Phys. Rev. Lett.* **97**, 083604 (2006).
- [54] Z. Wang, H. chun Yuan, and H. yi Fan, Nonclassicality of the photon addition-then-subtraction coherent state and its decoherence in the photon-loss channel, *J. Opt. Soc. Am. B* **28**, 1964 (2011).
- [55] S. M. Barnett, G. Ferenczi, C. R. Gilson, and F. C. Speirits, Statistics of photon-subtracted and photon-added states, *Phys. Rev. A* **98**, 013809 (2018).
- [56] S. Guerrini, M. Z. Win, and A. Conti, Photon-varied quantum states: Unified characterization, *Phys. Rev. A* **108**, 022425 (2023).
- [57] A. Zavatta, V. Parigi, M. S. Kim, and M. Bellini, Subtracting photons from arbitrary light fields: experimental test of coherent state invariance by single-photon annihilation, *New J. Phys.* **10**, 123006 (2008).
- [58] Y.-R. Chen, H.-Y. Hsieh, J. Ning, H.-C. Wu, H. L. Chen, Z.-H. Shi, P. Yang, O. Steuernagel, C.-M. Wu, and R.-K. Lee, Generation of heralded optical cat states by photon addition, *Phys. Rev. A* **110**, 023703 (2024).
- [59] M. M. Lund, F. Yang, V. R. Christiansen, D. Kornovan, and K. Mølmer, Subtraction and addition of propagating photons by two-level emitters, *Phys. Rev. Lett.* **133**, 103601 (2024).
- [60] K. Takase, J.-i. Yoshikawa, W. Asavanant, M. Endo, and A. Furusawa, Generation of optical schrödinger cat states by generalized photon subtraction, *Phys. Rev. A* **103**, 013710 (2021).
- [61] J.-P. Gazeau, *Coherent States in Quantum Physics* (Wiley-VCH, Berlin, 2009).
- [62] J. Weinbub and D. K. Ferry, Recent advances in wigner function approaches, *Appl. Phys. Rev.* **5**, 041104 (2018).
- [63] H. Yi Fan and H. Zaidi, Application of IWOP technique to the generalized Weyl correspondence, *Phys. Lett. A* **124**, 303 (1987).

- [64] V. Dodonov, I. Malkin, and V. Man'ko, Even and odd coherent states and excitations of a singular oscillator, *Physica* **72**, 597 (1974).
- [65] G. S. Thekkadath, B. A. Bell, I. A. Walmsley, and A. I. Lvovsky, Engineering Schrödinger cat states with a photonic even-parity detector, *Quantum* **4**, 239 (2020).
- [66] Su-Yong Lee, Chang-Woo Lee, Hyunchul Nha, and Dagomir Kaszlikowski, Quantum phase estimation using a multi-headed cat state, *J. Opt. Soc. Am. B* **32**, 1186 (2015).
- [67] J. Hastrup, J. S. Neergaard-Nielsen, and U. L. Andersen, Deterministic generation of a four-component optical cat state, *Opt. Lett.* **45**, 640 (2020).